

# Cross-attractor modeling of resting-state functional connectivity in psychiatric disorders reveals disturbances in excitation, inhibition, and energy gaps

Yinming Sun<sup>1</sup>, Mengsen Zhang<sup>2</sup>, Manish Saggar<sup>1</sup>

<sup>1</sup>Department of Psychiatry and Behavioral Sciences, Stanford University, Stanford, CA 94304

<sup>2</sup>Department of Psychiatry, University of North Carolina at Chapel Hill, Chapel Hill, NC 27514

## Abstract

Resting-state functional connectivity (RSFC) is altered across various psychiatric disorders. Biophysical network modeling (BNM) has the potential to reveal the neurobiological underpinnings of such abnormalities by dynamically modeling the structure-function relationship and examining biologically relevant parameters after fitting the models with real data. Although innovative BNM approaches have been developed, two main issues need to be further addressed. First, previous BNM approaches are primarily limited to simulating noise-driven dynamics near a chosen attractor (or a stable brain state). Such approaches miss out on the multi(or cross)-attractor dynamics that have been shown to better capture non-stationarity and switching between states in the resting brain. Second, previous BNM work is limited to characterizing one disorder at a time. Given the large degree of co-morbidity across psychiatric disorders, comparing BNMs across disorders might provide a novel avenue to generate insights regarding the dynamical features that are common across (vs. specific to) disorders. Here, we address these issues by (1) examining the layout of the attractor repertoire over the entire multi-attractor landscape using a recently developed cross-attractor BNM approach; and (2) characterizing and comparing multiple disorders (schizophrenia, bipolar, and ADHD) with healthy controls using an openly available and moderately large multimodal dataset from the UCLA Consortium for Neuropsychiatric Phenomics. Both global and local differences were observed across disorders. Specifically, the highest local excitation (across groups) was observed in the ADHD group, whereas the lowest local inhibition was observed in the bipolar group. In line with these results, the ADHD group had the lowest switching costs (energy gaps) across groups. Overall, this study provides preliminary evidence supporting transdiagnostic multi-attractor BNM approaches to better understand psychiatric disorders' pathophysiology.

## Introduction

Resting-state functional connectivity (RSFC) is observed to be altered across various psychiatric disorders, including schizophrenia, bipolar disorder, and attention deficit hyperactivity disorder (ADHD) (Baker et al., 2019; Friston et al., 2016; Khadka et al., 2013;

Konrad and Eickhoff, 2010; McCarthy et al., 2013; Perry et al., 2019; Xia et al., 2018). Likewise, structural connectivity (SC) based on diffusion-weighted imaging (DWI) has also revealed significant deviations across patient populations (Favre et al., 2019; Friston et al., 2016; Kelly et al., 2018; Konrad and Eickhoff, 2010; van Ewijk et al., 2012). Here, we argue for using a biophysical network modeling (BNM) approach that captures structure-function relationships to better characterize disorder-specific findings across modalities.

A vital benefit of the BNM approach is that it allows for examining differences in modeled physiological parameters (e.g., inhibitory synaptic strength) and generates concrete hypotheses regarding the neurobiological differences associated with psychiatric disorders. Along this line of thinking, previous studies have shown that RSFC can be partially predicted using SC directly or via modeling approaches (Hagmann et al., 2008; Honey et al., 2009; Kringelbach and Deco, 2020; Schirner et al., 2018). In terms of modeling psychiatric disorders, one BNM study with schizophrenia patients demonstrated how an increase in the regional excitation/inhibition (E/I) ratio led to an increase in functional connectivity, especially in the frontal-parietal network (Yang et al., 2016). Another study on autism patients showed that increased recurrent E/I explained abnormalities in both somatosensory regions and association cortices (Park et al., 2021). Finally, a study on ADHD patients found abnormalities in a model parameter linked to elevated regional oscillations and identified two subgroups of patients differing in personality traits (Iravani et al., 2021).

While previous modeling studies have advanced our understanding of psychiatric disorders, several key issues remain. First, previous applications of BNM in clinical populations were primarily limited to simulating noise-driven (or stochastic) dynamics near a chosen attractor (or a stable brain state; see (Cabral et al., 2017) for more details). Although such noise-driven exploration of a single attractor can capture critical features of the human resting-state dynamics (Deco et al., 2013; Demirtaş et al., 2019), multi(or cross)-attractor examination has been shown to better capture non-stationarity and switching between states in the resting brain (Freyer et al., 2012; Zhang et al., 2022). Second, previous BNM work was primarily limited to characterizing one disorder at a time. Given the large degree of co-morbidity across psychiatric disorders and the recent push in the field toward examining biological features across disorders, comparing BNMs across multiple disorders might provide a novel avenue to generate insights regarding the common dynamical features across disorders vs. specific to each disorder.

Here, we address both of these issues by (1) examining the layout of the attractor repertoire over the entire multi-attractor landscape using our recently developed cross-attractor BNM approach (Zhang et al., 2022); and (2) characterizing and comparing multiple disorders (schizophrenia, bipolar, and ADHD) with healthy controls using an openly available and moderately large multimodal dataset from the UCLA Consortium for Neuropsychiatric Phenomics (Poldrack et al., 2016).

Using data from undiagnosed adults from the Human Connectome Project (HCP), we have recently shown that relative to the models based on the noise-driven exploration of a single attractor, human RSFC can be more accurately explained by the set of possible transitions between all attractors, termed cross-attractor coordination matrix (Zhang et al., 2022).

Moreover, we also defined the concept of the “energy gap” between attractor states for characterizing the potential costs of state switching. Here, to capture individual differences in neurobiology across disorders, we varied model parameters for local excitation and inhibition and the global coupling between brain regions. The optimal individual combination of the parameters was determined based on how well the cross-attractor coordination matrix fits with the experimentally measured RSFC. Based on the optimal model configuration, we calculated the associated global energy gap measures for each subject following our previous study (Zhang et al., 2022). Since the abnormalities may localize to specific brain regions or functions, we also examined energy gap metrics averaged across regions of canonical resting-state networks (Yeo et al., 2011). The distribution of each model parameter and the global and network-specific energy gap measures were compared across the groups to identify disorder-specific abnormalities.

We expect the model fitness to be similar across participant groups. Based on previous findings of inhibitory neuron deficits, we hypothesize that parameters for local inhibition would be affected for schizophrenia and bipolar patients (Benes and Beretta, 2001; Lewis et al., 2012). We also expect higher values for energy gap measures in schizophrenia patients since they are associated with cognitive deficits and more severe psychopathology, which may result in more difficult transitions between attractor states. Regarding network-specific energy gap effects, we hypothesize the default mode network to show significant abnormalities given the large amount of evidence for its role in various psychiatric disorders (Baker et al., 2019; Bluhm et al., 2007; Whitfield-Gabrieli and Ford, 2012). Since ADHD has been associated with deficits in attention networks (McCarthy et al., 2013), we expect more significant abnormalities for energy gap metrics in the dorsal and ventral attention networks.

Overall, we aim to better characterize the commonality and differences between psychiatric disorders using a multi(cross)-attractor BNM and a transdiagnostic dataset.

## Methods

### Participants

The LA5c dataset was available through the OpenNeuro website, with further details presented elsewhere (Poldrack et al., 2016). In brief, adults ages 21 to 50 years were recruited from the Los Angeles area as part of the Consortium for Neuropsychiatric Phenomics. All participants gave informed consent and were either healthy (HLTY) or had a clinical diagnosis of schizophrenia (SCHZ), bipolar disorder (BPLR), or attention deficit hyperactivity disorder (ADHD). The downloaded dataset included 130 HLTY, 50 SCHZ, 49 BPLR, and 43 ADHD.

### Neuroimaging data description and analysis

The MRI data were collected using two 3T Siemens Trio scanners and included a 1 mm T1 scan with MPRAGE sequence, a 2 mm 64-direction DWI scan with one shell ( $b = 1000 \text{ s/mm}^2$ ),

and a 4 mm echo planar imaging (EPI) resting state fMRI (rsfMRI) scan with 2 s TRs and lasting 304 seconds.

rsfMRI was preprocessed using the automated workflow from fMRIprep, which is elaborated elsewhere (Esteban et al., 2019). The output fMRI in standard ‘MNI152NLin6Asym’ space was further processed by removing (censuring) volumes with a framewise displacement of 0.5 mm or higher, and regressing out six motion parameters (three translational and three rotational) from the remaining good frames. Any subject with less than 80% good frames was excluded from further analysis. To generate the RSFC, we used the Desikan-Killiany (DK) atlas for the parcellation (Desikan et al., 2006), which matches our previous study on HCP subjects and was shown to be a good choice in terms of runtime (Deco et al., 2013; Zhang et al., 2022). Whole brain rsfMRI timeseries were first averaged for voxels part of each parcel defined based on the subject DK atlas in standard ‘MNI152NLin6Asym’ space created via Freesurfer as part of the fMRIprep workflow. The parcel level timeseries were then correlated between each pair of parcels to generate the RSFC matrix.

For the analysis of diffusion scans, MRtrix3 was used for preprocessing, computing fixel-based values, and generating the probabilistic streamlines (Tournier et al., 2019). Preprocessing included removing random noise and ringing artifacts, removing distortion caused by eddy currents using the eddy functionality from FSL (Andersson et al., 2003), and applying bias field correction using the N4 algorithm of ANTs (Tustison et al., 2010). Subsequently, tissue response functions representing single-fiber white matter, gray matter, and cerebral spinal fluid (CSF) were computed and used for estimating the fiber orientation distribution (FOD) based on the multi-tissue constrained spherical deconvolution approach (Tournier et al., 2007). To generate an anatomically constrained tractography (ACT) (Smith et al., 2012), the structural T1 was co-registered to the DWI scan and was used to generate tissue segmentation of cortical gray matter, subcortical gray matter, white matter, CSF, and pathological tissue. Using the resulting tissue segmentations, 10 million probabilistic streamlines were generated with the MRtrix3 default iFOD2 algorithm by seeding at the gray and white matter interface. To remove biases in the whole-brain tract generation process, the number of streamlines was down-sampled to 1 million based on the SIFT algorithm (Smith et al., 2013). The co-registered subject-specific DK atlas was used to generate the SC by counting the number of streamlines between each parcel pair and normalizing by the average of the two parcel volumes. The resulting raw SC was further processed by setting the diagonal elements to zero and then normalizing by the value of the total connectivity from the parcel with the highest total connectivity (i.e., infinity normalized, Equation 4). For quality control based on outlier detection, the similarity between the SC of all subjects was quantified with Spearman’s correlation between the lower diagonal entries of the symmetrical matrix. Any subject with a similarity score of less than three standard deviations from the group mean was excluded from further analyses.

After excluding subjects with poor fMRI and outlier DWI connectivity, there were 104 HLTY, 29 SCHZ, 41 BPLR, and 31 ADHD participants. The demographics of the participants and their average framewise displacement (FD), are shown in Table 1. Significant group differences were observed for age, site (scanner), and average FD. Post-hoc, no significant paired comparison

difference was observed for the overall age effect (ANOVA F = 3.04, p = 0.03). For the overall site effect (Pearson's  $\chi^2 = 22.7$ , p < 0.001), the HLTY group had a larger percentage of participants from site 1 and a lower percentage from site 2 than expected (|standardized residuals| = 4.7). For the effect of average FD (ANOVA F = 5.21, p = 0.002), the HLTY group had a significantly lower value than both the SCHZ group (p = 0.008) and the BPLR group (p = 0.028).

**Table 1:** Participant demographics.

Group	N	Age*	Sex (Male/Female)	Site* (1/2)	Average Framewise Displacement (FD) *
Healthy (HLTY)	104	30.8±8.4	53/51	83/21	0.12±0.05
Schizophrenia (SCHZ)	29	34.7±9.5	22/7	15/14	0.16±0.05
Bipolar Disorder (BPLR)	41	35.0±8.4	22/19	21/20	0.15±0.07
Attention Deficit Hyperactivity Disorder (ADHD)	31	32.3±8.4	18/13	13/18	0.13±0.06

\* Significant group difference based on omnibus test

## Overview of the biophysical network model

The implementation details of our BNM model tailored for generating cross-attractor-based RSFC (Figure 1) have been presented elsewhere (Zhang et al., 2022). Briefly, the model has parameters that can be linked with biological quantities (i.e., an ensemble of leaky integrate-and-fire neurons receiving uncorrelated noisy inputs) as in the Wong-Wang model (Wong and Wang, 2006) and is modified such that the transfer function from input current to firing rate is similar to the Wilson-Cowan model (Wilson and Cowan, 1972), which captures a more diverse range of local dynamics.

Equations 1 and 2 describe how the synaptic activity of excitatory ( $S_E^{(i)}$ ) and inhibitory ( $S_I^{(i)}$ ) populations evolve in brain region  $i$ . For each region  $i$ ,  $w_{ab}^{(i)}$  represent the local coupling from population  $a$  to  $b$ ,  $H_p$  is the sigmoidal transfer function for population  $p$ ,  $I_G^{(i)}$  represent the global external input to the region  $i$  and  $\xi_p^{(i)}(t)$  is the intrinsic noise for population  $p$ . The decay time constants ( $\tau$ ), kinetic parameters ( $\gamma$ ), and noise scaling constant ( $\sigma$ ) are fixed for this study (see Table 2).

$$\frac{dS_E^{(i)}}{dt} = -\frac{S_E^{(i)}}{\tau_E} + (1 - S_E^{(i)})\gamma_E H_E(w_{EE}^{(i)}S_E^{(i)} - w_{IE}^{(i)}S_I^{(i)} + I_G^{(i)}(\overrightarrow{S_E})) + \sigma\xi_E^{(i)}(t) \quad (1)$$

$$\frac{dS_I^{(i)}}{dt} = -\frac{S_I^{(i)}}{\tau_I} + (1 - S_I^{(i)})\gamma_I H_I(w_{EI}^{(i)}S_E^{(i)} - w_{II}^{(i)}S_I^{(i)} + I_I) + \sigma\xi_I^{(i)}(t) \quad (2)$$

Equation 3 describes how the global input current ( $I_G^{(i)}$ ) to each region  $i$  is affected by the activity of all other regions  $j$ , which is scaled by the structural connectivity ( $C_{ij}$ ) and global coupling variable  $G$ . To generate  $C_{ij}$ , diagonal elements of the raw SC matrix were first set to 0. Then, the matrix elements were normalized by the maximum of the column sums (Equation 4).

$$I_G^{(i)}(\vec{S_E}) = G \sum_{j \neq i}^N C_{ij} S_E^{(j)} \quad (3)$$

$$\|C\|_\infty = \max_i (\sum_{j=1}^N |C_{ij}|) \equiv 1 \quad (4)$$

Equation 5 describes the sigmoidal transfer function for a neuronal population ( $p$ ), with constants  $a$ ,  $b$ ,  $d$ , and  $r_{max}$  defined in Table 2.

$$H_p(x) = \frac{r_{max} + \frac{a_p x - b_p - r_{max}}{1 - e^{-d_p(a_p x - b_p)}}}{1 - e^{-d_p(a_p x - b_p)}} \quad (5)$$

**Table 2: Fixed model parameter values.** For details on the choice of values, please refer to (Zhang et al., 2022) and previous literature (Deco et al., 2013; Wong and Wang, 2006).

Parameter	Value
$\tau_E$	0.1 (s)
$\tau_I$	0.01 (s)
$\gamma_E$	0.641
$\gamma_I$	1
$a_E$	310 (nC <sup>-1</sup> )
$b_E$	125 Hz
$d_E$	0.16 (s)
$a_I$	615 (nC <sup>-1</sup> )
$b_I$	177 (Hz)
$d_I$	0.087 (s)
$r_{max}$	500 (Hz)
$w_{II}$	0.05 (nA)
$I_I$	0.1 (nA)

## Computing attractor states

Due to the limited quality of the diffusion scans and previous studies showing the effectiveness of using a group average SC for the BNM modeling (Iravani et al., 2021; Zhang et al., 2022), we decided to use the group average SC for this study. Using a group-specific SC instead of one for all groups allowed for preserving group variations in SC in the subsequent analysis. The DK parcellation was chosen for comparison with previous works (Deco et al., 2013; Kringelbach and Deco, 2020; Zhang et al., 2022) and its optimal trade-off in terms of regional homogeneity and computational efficiency. Based on our previous work, a good local configuration of ( $w_{EE}$ ,  $w_{EI}$ )

for healthy subjects was observed at (2, 1) (Zhang et al., 2022). To allow patient groups to deviate in local configurations, nine different combinations of local parameters centered around (2, 1) were modeled.

Further, the global coupling parameter G was varied from 1 to 4 with 0.1 increments. The G range was set to capture all possible values for fitting individual differences in RSFC. In contrast, the increment size was set to minimize the number of run configurations but still be able to track the rate of change in the dynamic landscape. For each combination of parameters ( $G, w_{EE}, w_{EI}$ ), the set of fixed points was determined recursively by searching for steady-state solutions or zeroes from an initial set of guesses and then making new guesses based on the solutions found. The recursive process was repeated until a preset number of zeroes were found or a specific recursion depth limit was reached. Further details of the algorithm are presented in our previous work (Zhang et al., 2022). To determine the set of attractors from all the fixed points, we first classified the fixed points based on the Jacobian of the solution. We then performed an additional perturbation test around each fixed point for verification. Figures 1b and 1c show example bifurcation diagrams corresponding to each of the nine local configurations, with all the attractors labeled by type: stable nodes, stable spirals, and limit cycles. The remaining fixed points, labeled as others, are unstable and not attractors. Since the group average SC was used in this study, nine bifurcation diagrams (one for each local configuration), portraying all possible attractor states, were generated for each group.

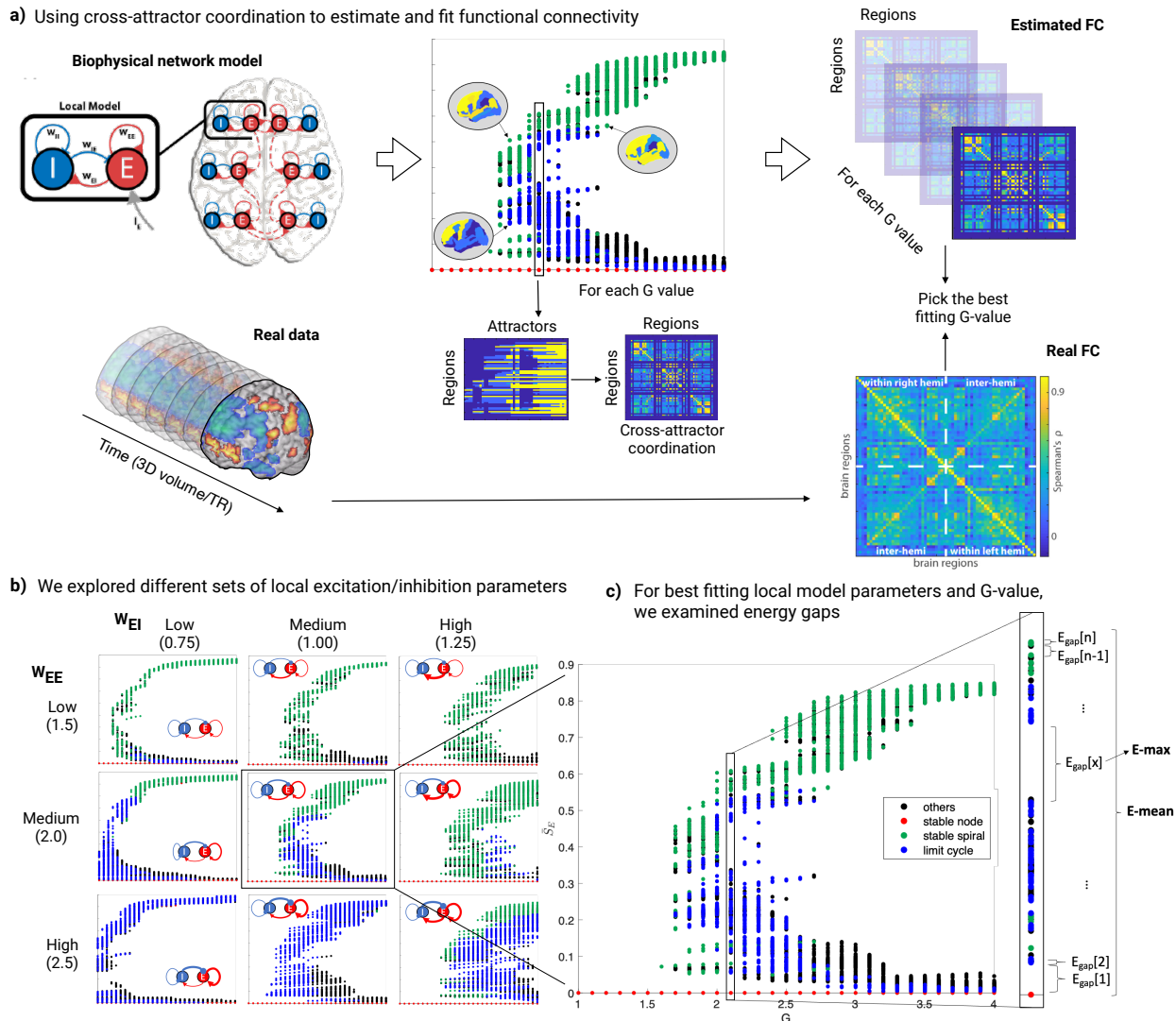


**Figure 1. Overview of cross-attractor-based model:** Panel a) shows how our model is used to estimate FC from the set of all attractors (i.e., cross-attractor coordination matrix), which is then fitted with real FC. Panel b) shows a set of bifurcation plots generated from nine different local configurations. Panel c) shows a zoomed-in version of one bifurcation plot to illustrate what the maximum and mean energy gap metrics ( $E_{max}$ ,  $E_{mean}$ ) represent.

## Individual RSFC fitting with cross-attractor coordination

The optimal configuration in terms of  $G$ ,  $w_{EE}$ , and  $w_{EI}$ , for each participant was determined by comparing the cross-attractor coordination matrix (Zhang et al., 2022) with the experimental RSFC (Figure 1a). For each combination of local parameters ( $w_{EE}$ ,  $w_{EI}$ ), the  $S_E$  values of each region across all attractors were first discretized based on the local maxima of the distribution and then correlated between each pair of model brain regions across all attractors, resulting in a square matrix with dimensions equaling to the number of parcellated regions. With the cross-attractor coordination matrix for each value of  $G$ , a similarity score with the measured RSFC

was calculated, which was used to determine the G associated with the most similar cross-attractor coordination matrix.

Since nine different local configurations ( $3 w_{EE} \times 3 w_{EI}$ ) were modeled with a G spanning between 1 and 4 and a step size of 0.1 (31 possibilities), the best fitting cross-attractor coordination matrix was found by comparing 279 model combinations. To prevent the fitting of RSFC to a cross-attractor coordination matrix associated with unrealistic attractor repertoires with large gaps between separate sub-repertoires, the maximum energy gap allowed for fitting was set to be no greater than 0.2 based on evidence from our previous work (Zhang et al., 2022).

## Energy gap calculations

Energy gap measures were calculated at the optimal (G,  $w_{EE}$ , and  $w_{EI}$ ) for each subject. Based on our previous study, the energy gap was defined by calculating the average  $S_E$  across all regions for each attractor and then taking the difference between adjacent attractors after sorting by the global average  $S_E$  values. The maximum and mean energy gap (E-max, E-mean) were then calculated from the distribution of energy gaps for each subject (Figure 1c). Since these measures were based on the global average  $S_E$ , we referred to them as global energy gap measures.

Additionally, we also examined network-specific energy gaps. Network-specific energy gaps between adjacent attractors were defined as the difference between the  $S_E$  averaged across brain regions that are part of specific canonical networks (Yeo et al., 2011). Each parcellated region of the DK atlas was assigned to a particular network based on which network had the most vertices in the region and included more than 25% of the vertices (Supplemental Figure 9a). The attractors were sorted based on the global  $S_E$  since attractor states themselves were defined based on the global average.

## Group comparison of individual values

The optimal G, the fitness correlation (Spearman's  $\rho$ ), E-max, and E-mean were compared across the clinical groups with the Kruskal-Wallis test after regressing out covariates for age, sex, site (scanner), and average FD. Post-hoc rank-sum tests with Tukey correction were used to determine significant paired differences if there was an overall group effect. Non-linear tests were used since the distributions of the variables were not normal.

For comparing the distribution of optimal  $w_{EE}$  and  $w_{EI}$  between the groups, a Pearson's  $\chi^2$  test was used to compare the proportions of subjects in each configuration across the groups. The comparison was done for  $w_{EE}$  and  $w_{EI}$  separately. If there was an overall effect, the standardized residuals (i.e., absolute value > 3) were used to determine which configuration had a proportion that contributed the most to the effect (Sharpe, 2015).

## Results

### Description of attractor landscapes

The bifurcation diagram of  $S_E$  with changing values of  $G$  agrees with previous studies (Deco et al., 2013; Zhang et al., 2022). Key characteristics include an initial jump from a single stable state to multiple stable states or multistability, and a second bifurcation that splits the set of attractors to a lower and higher arm (Figure 1). The arms then gradually collapse toward two extreme states with further increases in  $G$ .

The nine bifurcation diagrams for each participant group are shown in Supplemental Figures 1 to 4. To better illustrate how the landscape changes in attractor type and numbers, Supplemental Figures 5 to 8 show the total number of attractors and the number of attractors of each type for each group. As  $w_{EE}$  increases, the gap between the first and second major bifurcation value of  $G$  is widened. The attractors also span a wider range of  $S_E$  values for higher  $G$  values. As  $w_{EI}$  increases, the entire bifurcation diagram shifts toward a higher  $G$ , including the  $G$  value at the first and second major bifurcation. The total number of possible attractors across all  $G$  increases while the number of limit cycle solutions decreases and occurs at higher  $G$  values.

### Individual model fitting similar across groups

Figure 2a shows the distribution of correlation (Spearman's  $\rho$ ) between the cross-attractor coordination matrix and real RSFC for each participant group. The individual fitting of model parameters resulted in very similar correlation values for each of the 4 groups, which were 0.41 (0.09) for HLTY, 0.45 (0.08) for SCHZ, 0.43 (0.11) for BPLR, and 0.39 (0.09) for ADHD. Overall, model fitting was at par with previous studies (Deco et al., 2013; Iravani et al., 2021; Park et al., 2021; Wang et al., 2019). Example fitting results for selected participants are shown in Supplemental Figures 11 to 14. After regressing out the effect of age, sex, site (scanner), and average FD, there was no significant group effect for the fitness correlation based on a 1-way Kruskal-Wallis test ( $\chi^2 = 4.92$ ,  $p = 0.18$ ).

The distribution of optimal  $G$  associated with correlation values is shown in Figure 2b. The average  $G$  value was 2.6 (0.5) for HLTY, 2.3 (0.4) for SCHZ, 2.2 (0.6) for BPLR, and 2.4 (0.5) for ADHD. These values are close to where the fitted bifurcation diagram starts to split into a high and low sub-repertoire of attractors, or what Deco and colleagues refer to as the edge of the second bifurcation or criticality (Deco et al., 2013). It is also where the total number of attractors is typically the largest (see Supplemental Figures 1-8). After regressing out the effect of age, sex, site (scanner), and average framewise displacement, there was a significant group effect for the optimal  $G$  based on a 1-way Kruskal-Wallis test ( $\chi^2 = 7.62$ ,  $p = 0.05$ ). No rank-sum paired comparisons were significant after correction for multiple comparisons.

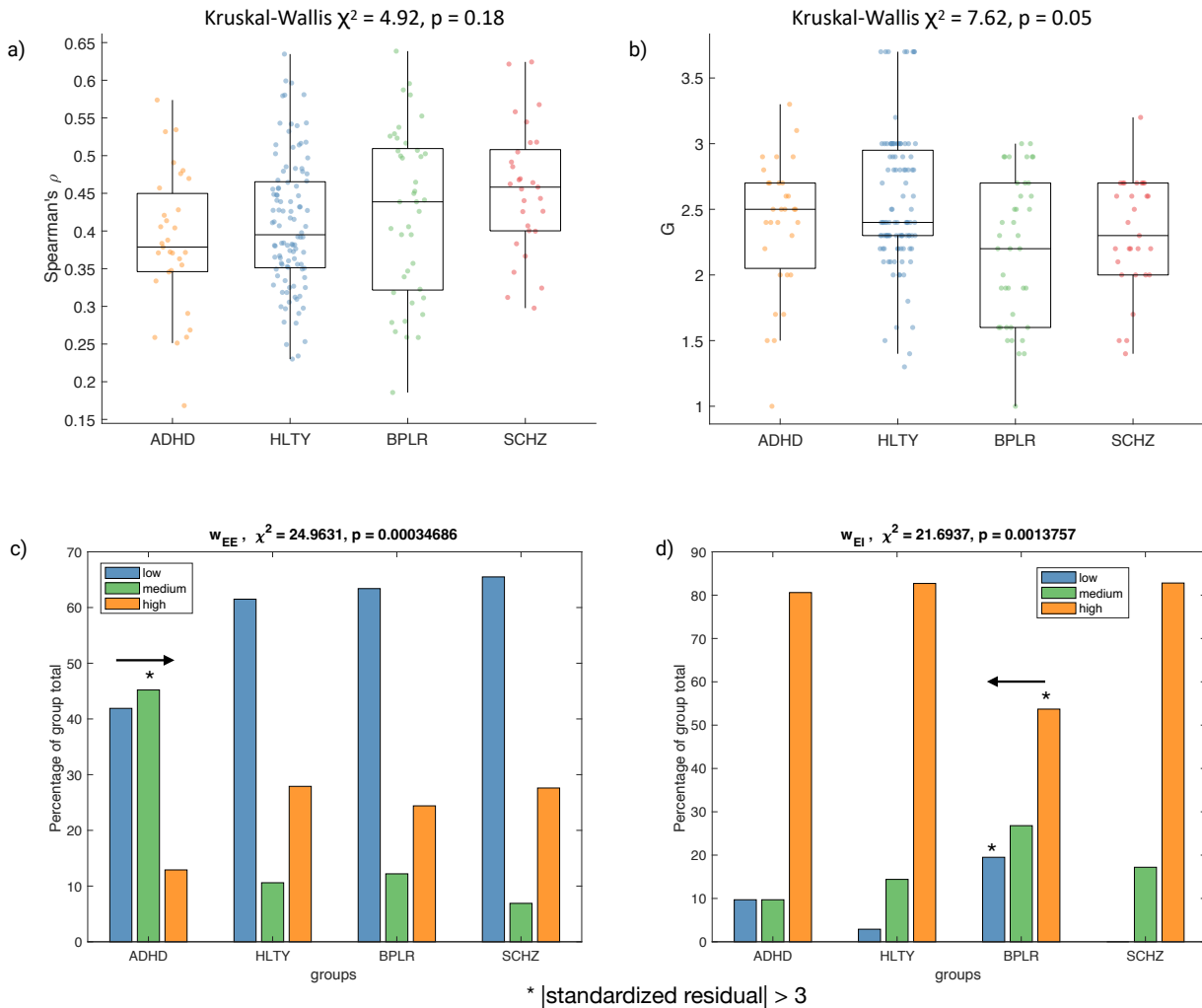


**Figure 2. Model parameter fitting:** Boxplots showing the distribution of a) model fitness (Spearman's  $\rho$ ), and b) global coupling ( $G$ ) value. The Kruskal-Wallis test results are shown for group comparisons after controlling for age, sex, site, and average FD. Bar plots show the distribution of local parameters c)  $w_{EE}$  and d)  $w_{EI}$  for each participant group. Pearson's  $\chi^2$  test results are significant for both local parameters. Based on standardized residuals, the ADHD group shows an increase in medium  $w_{EE}$  proportions, while the BPLR group shows a decrease in high  $w_{EI}$  proportions and an increase in low  $w_{EI}$  proportions. The arrows help to illustrate the direction of change.

## Optimal local configuration differs across groups

The optimal local configuration in terms of  $(w_{EE}, w_{EI})$  is  $(1.5, 1.25)$  for all the groups except for ADHD, which has a higher prevalence of  $(2, 1.25)$ . Figure 2c shows the proportion of participants with low (1.5), medium (2.0), and high (2.5) values of  $w_{EE}$  for each of the groups, while Figure 2d shows the low (0.75), medium (1.00), and high (1.25) values of  $w_{EI}$ . A test of proportions shows that the distribution of participants across the possible  $w_{EE}$  values were significantly different from the expected (Pearson  $\chi^2 = 25.0$ ,  $p = 0.0003$ ), with the ADHD group having a higher proportion of medium  $w_{EE}$  (standardized residuals = 4.9). Likewise, a test of

proportions shows that the distribution of participants across the possible  $w_{EI}$  values were also significantly different from the expected ( $\chi^2 = 21.7$ ,  $p = 0.001$ ), with the bipolar group having a proportion of low  $w_{EI}$  being higher (standardized residuals = 3.6) and a proportion of high  $w_{EI}$  being lower (standardized residuals = -3.9).

## The global energy gap differs across groups

The distribution of the global E-max is shown in Figure 3a. The group average E-max was 0.11 (0.05) for HLTY, 0.11 (0.04) for SCHZ, 0.13 (0.05) for BPLR, and 0.09 (0.04) for ADHD. The distribution of global E-mean is shown in Supplemental Figure 10a. The group average E-mean was 0.014 (0.008) for HLTY, 0.015 (0.015) for SCHZ, 0.016 (0.011) for BPLR, and 0.013 (0.013) for ADHD (Supplemental Figure 10a). After regressing out the effect of age, sex, site (scanner), and average FD, there was a significant group effect based on a 1-way Kruskal-Wallis test for E-max ( $\chi^2 = 8.08$ ,  $p = 0.04$ ) and E-mean ( $\chi^2 = 9.13$ ,  $p = 0.02$ ). Post-hoc rank-sum tests show that E-max was significantly higher in the BPLR group than the ADHD group, while E-mean was significantly higher in the HLTY group than the ADHD group.

## Network specific energy gap differs across groups

As an exploratory analysis, the DK atlas parcels were assigned into the 7 canonical networks (Supplemental Figure 9a). Significant group differences in terms of E-max and E-mean were present for certain networks, with changes not necessarily in the same direction. E-max comparison results for the default mode network and frontal parietal network are shown in Figure 3b and 3c respectively. Results for all networks are shown in Supplemental Figure 9 for E-max, and Supplemental Figure 10 for E-mean.

Significant overall group differences in terms of E-max were found for: 1) the default mode network ( $\chi^2 = 8.23$ ,  $p = 0.04$ ), which has a significantly higher value for SCHZ than ADHD; 2) the dorsal attention network ( $\chi^2 = 21.5$ ,  $p = 8 \times 10^{-5}$ ), which has a significantly lower value for ADHD than all the other groups; and 3) the visual network ( $\chi^2 = 8.49$ ,  $p = 0.04$ ), which has a significantly lower value for the SCHZ group than the HLTY and BPLR groups.

Significant overall group differences in terms of E-mean were found for most of the networks including the default mode network ( $\chi^2 = 9.14$ ,  $p = 0.03$ ), the frontal parietal network ( $\chi^2 = 10.8$ ,  $p = 0.01$ ), the ventral attention network ( $\chi^2 = 12.2$ ,  $p = 0.007$ ), the dorsal attention network ( $\chi^2 = 7.77$ ,  $p = 0.05$ ), the somatomotor network ( $\chi^2 = 8.11$ ,  $p = 0.04$ ), and the visual network ( $\chi^2 = 8.11$ ,  $p = 0.04$ ). Post-hoc rank-sum tests show that the HLTY group has a significantly higher value than the ADHD group for all the aforementioned networks, except for the somatomotor network, which has no significant paired difference, and the ventral attention network, which has a significantly higher value for the HLTY group than the SCHZ group.

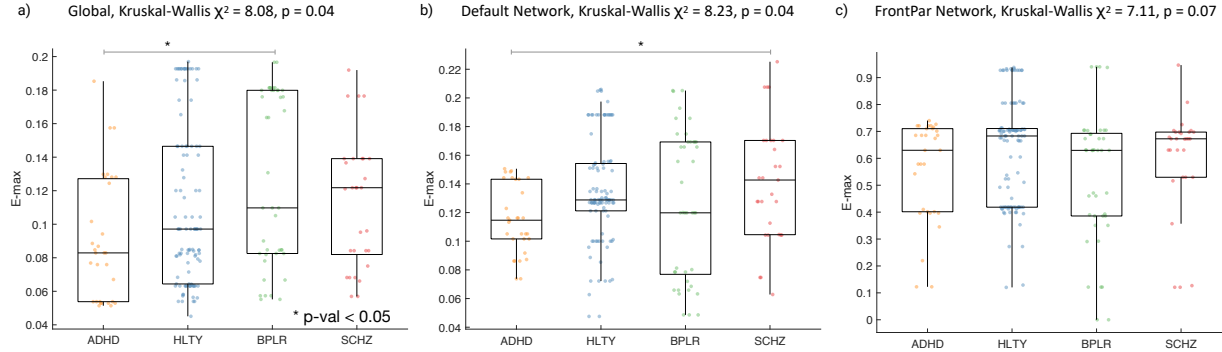


**Figure 3. Energy gap metrics:** Boxplots showing group E-max distributions when values are a) global, or restricted to the b) default mode network, and c) frontal parietal network. The Kruskal-Wallis test results are shown for group comparisons after controlling for age, sex, site, and average FD. There are main group effects for global and default mode network E-max, but not frontal parietal network E-max. Post hoc comparisons show larger global E-max in the BPLR group than ADHD group, and larger default mode network E-max in the SCHZ group than ADHD group.

## Examining correlation with clinical symptoms

Given the significant group differences in specific local parameters and energy gap metrics, we sought to determine if they were linked with specific symptoms while controlling for age, sex, site (scanner), and average FD. For ADHD participants, we correlated their  $w_{EE}$  and global E-max values with their hyperactivity and attention total scores on the Adult ADHD Clinical Diagnostic Scale (ACDS). For BPLR participants, we correlated their  $w_{EI}$  and global E-max values with their total score on the Young's Mania Rating Scale (YMRS) and their total score on the 17-items Hamilton Depression Rating Scale (HAMD-17). No significant correlations were found after correction for multiple comparisons.

## Discussion

Our results demonstrated that psychiatric disorders might be characterized by disturbances in the brain's attractor landscape described by our BNM model. This was shown through significant group effects for the global coupling and local parameters for excitation and inhibition, as well as the maximum global energy gap associated with the optimal individual parameters. Further insight was revealed by comparing energy gap metrics for specific resting state networks, including more accentuated abnormalities in the default mode network and dorsal attention network.

## Model fitting performance across psychiatric populations

The level of fit between the estimated RSFC (i.e. cross-attractor coordination matrix) and the real RSFC was similar across the groups. The level of correlation is comparable to previous BNM studies (Deco et al., 2013; Iravani et al., 2021; Park et al., 2021; Wang et al., 2019), suggesting that the model fitting procedure works well for patient populations.

There was an overall group effect for the global coupling G, with the healthy group having the highest ( $G = 2.6$ ), followed by ADHD ( $G = 2.4$ ) and schizophrenia ( $G = 2.3$ ) groups, and with the bipolar group having the lowest ( $G = 2.2$ ). While no post-hoc paired comparisons were significant after correction for multiple comparisons, the overall group effect suggests that psychopathology may be partly due to changes in the global coupling modulating connections between all regions. A recent study argued that global coupling could be considered a factor for operationalizing the balance between local and global influences on a brain region, such that a decrease in global coupling could result in less (or more) global (or local) influence (Klein et al., 2021). This is consistent with the disconnection hypothesis (Friston et al., 2016) for schizophrenia and the related psychosis of interoception for bipolar patients (Perry et al., 2019), which both refer to a disruption of normal large-scale brain network dynamics.

## Differences in local excitation and inhibition across populations

The optimal local configuration of ( $w_{EE}$ ,  $w_{EI}$ ) across all groups was (1.5, 1.25). The attractor landscape was dominated by stable spirals or damped oscillations (see Supplemental Figures 1-8). While the reasoning for this observation may require further theoretical exploration, one possibility is that the ongoing activity of the resting state brain is a summation of damped oscillatory processes (Evertz et al., 2022), which can arise from spontaneous transitions between the available stable spiral attractors.

Relative to the other groups, the ADHD group had a significantly higher proportion of individuals with the middle  $w_{EE} = 2.0$ , which suggests that local excitation was higher for subjects in the group (Figure 2c). This agrees with previous findings showing that the overactivation of pyramidal neurons in the cortex can cause ADHD symptomatology (Arnsten, 2009). Increasing local excitation causes the number of attractors to increase and the energy gap between adjacent attractors to decrease, especially for lower G values, resulting in easier or perhaps excessive state transitions.

Relative to the other groups, the bipolar group had a significantly higher proportion of individuals with the lower  $w_{EI} = 0.75$ , and lower proportion of individuals with the higher  $w_{EI} = 1.25$ , suggesting that local inhibition was abnormally low in the group (Figure 2d). Our finding agrees with previous cellular studies showing impaired inhibitory neurotransmission across the brain in the group (Benes and Berretta, 2001; Lee et al., 2018). Moreover, an increase in the E/I ratio, which can result from decreased inhibition, has been associated with bipolar disorders, while restoration of that imbalance has been linked to the mood-stabilizing effect of lithium treatment (Khayachi et al., 2021; Lee et al., 2018). The fact that the inhibitory deficits were not found in the schizophrenia group is slightly surprising given the shared and often more severe inhibitory deficits (Benes and Berretta, 2001). This lack of result could be due to stronger but more localized impairments in schizophrenia. Future work with a heterogeneous BNM approach (with different local parameter values across brain regions) might be better suited to capture such localized differences.

Decreased inhibition also causes the onset of multistability to occur with less global coupling (see Supplemental Figures 1-8). Since the set of attractors split into two repertoires, bifurcation

of brain states with less required global coupling may explain why bipolar patients are associated with two alternating pathological modes, one of depression and one of mania.

While abnormally high excitation, as in the case of ADHD, and unusually low inhibition, as in the case of bipolar disorder, both lead to an increase in the E/I balance, the underlying deficit can arise from different sources, as shown. Therefore, future studies should consider the source of the imbalance (i.e., numerator or denominator) in addition to the ratio itself.

### Implications of abnormal energy gap metrics and brain state transitions

Overall, there was a group effect for E-max and E-mean. While E-max mostly tracks larger gaps between potential sub-repertoires of attractors, E-mean mostly tracks the density of attractors. The significant group differences in global energy gap measures point to differences in the brain's ability to switch between different brain states.

Relative to the healthy group, the ADHD group had lower E-max and E-mean values, while the bipolar group had higher values. An abnormally low E-max and E-mean allows for easier transitions between attractor states within and between potential sub-repertoires. In contrast, an unusually high E-max or E-mean makes specific transitions less probable, putatively leading to higher dwelling of a few states. This concept has been examined through microstate transition probabilities and occurrences, which have been shown to be abnormal for ADHD (Férat et al., 2021) and bipolar patients (Damborská et al., 2019).

At the network level, the ADHD group also showed a lower E-max for the dorsal attention network relative to all other groups. The group also showed a lower E-mean relative to healthy controls in the default mode, frontal-parietal, dorsal attention, and visual networks. Abnormal state transitions in the dorsal attention and frontal-parietal networks have been shown in the ADHD population in previous microstate studies (Férat et al., 2021; Luo et al., 2021). Based on RSFC studies, the ADHD group has been associated with decreased connectivity in the attention networks and increased connectivity in the default mode network (McCarthy et al., 2013). Since the global coupling was set to be the same for all parcels in this study, the network-specific deviations may have been reflected in the energy gap metrics.

The schizophrenia group had the highest E-max for the default mode network, which was significantly higher than the ADHD group. Many studies have shown default mode network abnormalities in schizophrenia patients (Bluhm et al., 2007; Ongür et al., 2010; Whitfield-Gabrieli and Ford, 2012). The higher E-max may lead to positive or negative symptoms associated with inefficient transitions involving the default mode network (Al Zoubi et al., 2019; da Cruz et al., 2020). The schizophrenia group also had a significantly lower E-mean for the visual network and lower E-max for the ventral attention network relative to healthy controls, and a significantly lower E-max for the visual network relative to the bipolar group. Lower E-max for the visual network may cause abnormal visual system activation, which could also lead to positive symptoms (Li et al., 2017). Given that no significant abnormalities for the schizophrenia group were shown with the global energy gap metrics, these findings suggest more network-specific abnormalities in the population.

## Limitations and future directions

While the results of this study showed the promise of our modeling approach for understanding psychiatric disorders, there are several limitations. First, the sample size is small, especially for the patient groups. Therefore, replication of the results in a larger and independent sample is necessary. Nevertheless, given that the purpose of this study was to demonstrate the utility of the cross-attractor modeling approach in patient populations, the immediate goal was achieved. Second, the quality of the DWI and rsfMRI scans was poor, especially relative to the quality of HCP scans, which is likely why the model fitness values for the groups were slightly lower than reported for the sample of HCP subjects in our previous study (Zhang et al., 2022). While our model was able to draw helpful conclusions from the clinical grade scans, refinement of the model will benefit from having higher quality scans for patient populations. Third, the model did not allow the local parameters to vary between regions. The assumption of uniform configurations across the brain had been made in most BNM studies due to computational limitations and the risk of overfitting (Deco et al., 2013; Schirner et al., 2018). Future studies with optimization approaches built for high dimensional fitting problems, such as evolutionary optimization (Maile et al., 2019; Miikkulainen, 2021), may help to overcome this challenge.

## Acknowledgements

This work was supported by a NIH Director's New Innovator Award (MH119735) and a Stanford MCHRI Faculty Scholar Award to M.S.

## References

- Al Zoubi, O., Mayeli, A., Tsuchiyagaito, A., Misaki, M., Zotev, V., Refai, H., Paulus, M., Bodurka, J., Tulsa 1000 Investigators, 2019. EEG Microstates Temporal Dynamics Differentiate Individuals with Mood and Anxiety Disorders From Healthy Subjects. *Front. Hum. Neurosci.* 13, 56.
- Andersson, J.L.R., Skare, S., Ashburner, J., 2003. How to correct susceptibility distortions in spin-echo echo-planar images: application to diffusion tensor imaging. *Neuroimage* 20, 870–888.
- Arnsten, A.F.T., 2009. The Emerging Neurobiology of Attention Deficit Hyperactivity Disorder: The Key Role of the Prefrontal Association Cortex. *J. Pediatr.* 154, I-S43.
- Baker, J.T., Dillon, D.G., Patrick, L.M., Roffman, J.L., Brady, R.O., Jr, Pizzagalli, D.A., Öngür, D., Holmes, A.J., 2019. Functional connectomics of affective and psychotic pathology. *Proc. Natl. Acad. Sci. U. S. A.* 116, 9050–9059.
- Benes, F.M., Beretta, S., 2001. GABAergic interneurons: implications for understanding schizophrenia and bipolar disorder. *Neuropsychopharmacology* 25, 1–27.
- Bluhm, R.L., Miller, J., Lanius, R.A., Osuch, E.A., Bokslan, K., Neufeld, R.W.J., Théberge, J., Schaefer, B., Williamson, P., 2007. Spontaneous low-frequency fluctuations in the BOLD signal in schizophrenic patients: anomalies in the default network. *Schizophr. Bull.* 33, 1004–1012.
- Cabral, J., Krriegelbach, M.L., Deco, G., 2017. Functional connectivity dynamically evolves on multiple time-scales over a static structural connectome: Models and mechanisms. *Neuroimage* 160, 84–96.
- da Cruz, J.R., Favrod, O., Roinishvili, M., Chkonia, E., Brand, A., Mohr, C., Figueiredo, P., Herzog, M.H., 2020. EEG microstates are a candidate endophenotype for schizophrenia. *Nat. Commun.* 11, 3089.
- Damborská, A., Piguet, C., Aubry, J.-M., Dayer, A.G., Michel, C.M., Berchio, C., 2019. Altered Electroencephalographic Resting-State Large-Scale Brain Network Dynamics in Euthymic Bipolar Disorder Patients. *Front. Psychiatry* 10, 826.
- Deco, G., Ponce-Alvarez, A., Mantini, D., Romani, G.L., Hagmann, P., Corbetta, M., 2013. Resting-state functional connectivity emerges from structurally and dynamically shaped slow linear fluctuations. *J. Neurosci.* 33, 11239–11252.
- Demirtaş, M., Burt, J.B., Helmer, M., Ji, J.L., Adkinson, B.D., Glasser, M.F., Van Essen, D.C., Sotiropoulos, S.N., Anticevic, A., Murray, J.D., 2019. Hierarchical heterogeneity across human cortex shapes large-scale neural dynamics. *Neuron* 101, 1181-1194.e13.
- Desikan, R.S., Ségonne, F., Fischl, B., Quinn, B.T., Dickerson, B.C., Blacker, D., Buckner, R.L., Dale, A.M., Maguire, R.P., Hyman, B.T., Albert, M.S., Killiany, R.J., 2006. An automated labeling system for subdividing the human cerebral cortex on MRI scans into gyral based regions of interest. *Neuroimage* 31, 968–980.
- Esteban, O., Markiewicz, C.J., Blair, R.W., Moodie, C.A., Isik, A.I., Erramuzpe, A., Kent, J.D., Goncalves, M., DuPre, E., Snyder, M., Oya, H., Ghosh, S.S., Wright, J., Duriez, J., Poldrack, R.A., Gorgolewski, K.J., 2019. fMRIprep: a robust preprocessing pipeline for functional MRI. *Nat. Methods* 16, 111–116.
- Evertz, R., Hicks, D.G., Liley, D.T.J., 2022. Alpha blocking and  $1/f\beta$  spectral scaling in resting EEG can be accounted for by a sum of damped alpha band oscillatory processes. *PLoS Comput. Biol.* 18, e1010012.
- Favre, P., Pauling, M., Stout, J., Hozer, F., Sarrazin, S., Abé, C., Alda, M., Alloza, C., Alonso-Lana, S., Andreassen, O.A., Baune, B.T., Benedetti, F., Busatto, G.F., Canales-Rodríguez, E.J., Caseras, X., Chaim-Avancini, T.M., Ching, C.R.K., Dannlowski, U.,

- Deppe, M., Eyler, L.T., Fatjo-Vilas, M., Foley, S.F., Grotegerd, D., Hajek, T., Haukvik, U.K., Howells, F.M., Jahanshad, N., Kugel, H., Lagerberg, T.V., Lawrie, S.M., Linke, J.O., McIntosh, A., Melloni, E.M.T., Mitchell, P.B., Polosan, M., Pomarol-Clotet, E., Repple, J., Roberts, G., Roos, A., Rosa, P.G.P., Salvador, R., Sarró, S., Schofield, P.R., Serpa, M.H., Sim, K., Stein, D.J., Sussmann, J.E., Temmingh, H.S., Thompson, P.M., Verdolini, N., Vieta, E., Wessa, M., Whalley, H.C., Zanetti, M.V., Leboyer, M., Mangin, J.-F., Henry, C., Duchesnay, E., Houenou, J., ENIGMA Bipolar Disorder Working Group, 2019. Widespread white matter microstructural abnormalities in bipolar disorder: evidence from mega- and meta-analyses across 3033 individuals. *Neuropsychopharmacology* 44, 2285–2293.
- Férat, V., Arns, M., Deiber, M.-P., Hasler, R., Perroud, N., Michel, C.M., Ros, T., 2021. Electroencephalographic Microstates as Novel Functional Biomarkers for Adult Attention-Deficit/Hyperactivity Disorder. *Biol Psychiatry Cogn Neurosci Neuroimaging*. <https://doi.org/10.1016/j.bpsc.2021.11.006>
- Freyer, F., Roberts, J.A., Ritter, P., Breakspear, M., 2012. A canonical model of multistability and scale-invariance in biological systems. *PLoS Comput. Biol.* 8, e1002634.
- Friston, K., Brown, H.R., Siemerkus, J., Stephan, K.E., 2016. The dysconnection hypothesis (2016). *Schizophr. Res.* 176, 83–94.
- Hagmann, P., Cammoun, L., Gigandet, X., Meuli, R., Honey, C.J., Wedeen, V.J., Sporns, O., 2008. Mapping the Structural Core of Human Cerebral Cortex. *PLoS Biology*. <https://doi.org/10.1371/journal.pbio.0060159>
- Honey, C.J., Sporns, O., Cammoun, L., Gigandet, X., Thiran, J.P., Meuli, R., Hagmann, P., 2009. Predicting human resting-state functional connectivity from structural connectivity. *Proceedings of the National Academy of Sciences*. <https://doi.org/10.1073/pnas.0811168106>
- Iravani, B., Arshamian, A., Fransson, P., Kaboodvand, N., 2021. Whole-brain modelling of resting state fMRI differentiates ADHD subtypes and facilitates stratified neuro-stimulation therapy. *Neuroimage* 231, 117844.
- Kelly, S., Jahanshad, N., Zalesky, A., Kochunov, P., Agartz, I., Alloza, C., Andreassen, O.A., Arango, C., Banaj, N., Bouix, S., Bousman, C.A., Brouwer, R.M., Bruggemann, J., Bustillo, J., Cahn, W., Calhoun, V., Cannon, D., Carr, V., Catts, S., Chen, J., Chen, J.-X., Chen, X., Chiapponi, C., Cho, K.K., Ciullo, V., Corvin, A.S., Crespo-Facorro, B., Cropley, V., De Rossi, P., Diaz-Caneja, C.M., Dickie, E.W., Ehrlich, S., Fan, F.-M., Faskowitz, J., Fatouros-Bergman, H., Flyckt, L., Ford, J.M., Fouche, J.-P., Fukunaga, M., Gill, M., Glahn, D.C., Gollub, R., Goudzwaard, E.D., Guo, H., Gur, R.E., Gur, R.C., Gurholt, T.P., Hashimoto, R., Hatton, S.N., Henskens, F.A., Hibar, D.P., Hickie, I.B., Hong, L.E., Horacek, J., Howells, F.M., Hulshoff Pol, H.E., Hyde, C.L., Isaev, D., Jablensky, A., Jansen, P.R., Janssen, J., Jönsson, E.G., Jung, L.A., Kahn, R.S., Kikinis, Z., Liu, K., Klauser, P., Knöchel, C., Kubicki, M., Lagopoulos, J., Langen, C., Lawrie, S., Lenroot, R.K., Lim, K.O., Lopez-Jaramillo, C., Lyall, A., Magnotta, V., Mandl, R.C.W., Mathalon, D.H., McCarley, R.W., McCarthy-Jones, S., McDonald, C., McEwen, S., McIntosh, A., Melicher, T., Mesholam-Gately, R.I., Michie, P.T., Mowry, B., Mueller, B.A., Newell, D.T., O'Donnell, P., Oertel-Knöchel, V., Oestreich, L., Paciga, S.A., Pantelis, C., Pasternak, O., Pearson, G., Pellicano, G.R., Pereira, A., Pineda Zapata, J., Piras, F., Potkin, S.G., Preda, A., Rasser, P.E., Roalf, D.R., Roiz, R., Roos, A., Rotenberg, D., Satterthwaite, T.D., Savadjiev, P., Schall, U., Scott, R.J., Seal, M.L., Seidman, L.J., Shannon Weickert, C., Whelan, C.D., Shenton, M.E., Kwon, J.S., Spalletta, G., Spaniel, F., Sprooten, E., Stäblein, M., Stein, D.J., Sundram, S., Tan, Y., Tan, S., Tang, S., Temmingh, H.S., Westlye, L.T., Tønnesen, S., Tordesillas-Gutierrez, D., Doan, N.T., Vaidya, J., van Haren, N.E.M., Vargas, C.D., Vecchio, D., Velakoulis, D., Voineskos, A., Voyvodic, J.Q., Wang, Z., Wan, P., Wei, D., Weickert, T.W., Whalley, H., White, T., Whitford, T.J.,

- Wojcik, J.D., Xiang, H., Xie, Z., Yamamori, H., Yang, F., Yao, N., Zhang, G., Zhao, J., van Erp, T.G.M., Turner, J., Thompson, P.M., Donohoe, G., 2018. Widespread white matter microstructural differences in schizophrenia across 4322 individuals: results from the ENIGMA Schizophrenia DTI Working Group. *Mol. Psychiatry* 23, 1261–1269.
- Khadka, S., Meda, S.A., Stevens, M.C., Glahn, D.C., Calhoun, V.D., Sweeney, J.A., Tamminga, C.A., Keshavan, M.S., O’Neil, K., Schretlen, D., Pearlson, G.D., 2013. Is aberrant functional connectivity a psychosis endophenotype? A resting state functional magnetic resonance imaging study. *Biol. Psychiatry* 74, 458–466.
- Khayachi, A., Ase, A., Liao, C., Kamesh, A., Kuhlmann, N., Schorova, L., Chaumette, B., Dion, P., Alda, M., Séguéla, P., Rouleau, G., Milnerwood, A., 2021. Chronic lithium treatment alters the excitatory/inhibitory balance of synaptic networks and reduces mGluR5-PKC signalling in mouse cortical neurons. *J. Psychiatry Neurosci.* 46, E402–E414.
- Klein, P.C., Ettinger, U., Schirner, M., Ritter, P., Rujescu, D., Falkai, P., Koutsouleris, N., Kambeitz-Ilankovic, L., Kambeitz, J., 2021. Brain network simulations indicate effects of neuregulin-1 genotype on excitation-inhibition balance in cortical dynamics. *Cereb. Cortex* 31, 2013–2025.
- Konrad, K., Eickhoff, S.B., 2010. Is the ADHD brain wired differently? A review on structural and functional connectivity in attention deficit hyperactivity disorder. *Hum. Brain Mapp.* 31, 904–916.
- Kringelbach, M.L., Deco, G., 2020. Brain States and Transitions: Insights from Computational Neuroscience. *Cell Rep.* 32, 108128.
- Lee, Y., Zhang, Y., Kim, S., Han, K., 2018. Excitatory and inhibitory synaptic dysfunction in mania: an emerging hypothesis from animal model studies. *Exp. Mol. Med.* 50, 1–11.
- Lewis, D.A., Curley, A.A., Glausier, J.R., Volk, D.W., 2012. Cortical parvalbumin interneurons and cognitive dysfunction in schizophrenia. *Trends in Neurosciences.* <https://doi.org/10.1016/j.tins.2011.10.004>
- Li, P., Fan, T.-T., Zhao, R.-J., Han, Y., Shi, L., Sun, H.-Q., Chen, S.-J., Shi, J., Lin, X., Lu, L., 2017. Altered Brain Network Connectivity as a Potential Endophenotype of Schizophrenia. *Sci. Rep.* 7, 5483.
- Luo, N., Luo, X., Yao, D., Calhoun, V.D., Sun, L., Sui, J., 2021. Investigating ADHD subtypes in children using temporal dynamics of the electroencephalogram (EEG) microstates. *Conf. Proc. IEEE Eng. Med. Biol. Soc.* 2021, 4358–4361.
- Maile, K., Saggar, M., Miikkulainen, R., 2019. Implementing evolutionary optimization to model neural functional connectivity, in: Proceedings of the Genetic and Evolutionary Computation Conference Companion on - GECCO ’19. Presented at the the Genetic and Evolutionary Computation Conference Companion, ACM Press, New York, New York, USA. <https://doi.org/10.1145/3319619.3326826>
- McCarthy, H., Skokauskas, N., Mulligan, A., Donohoe, G., Mullins, D., Kelly, J., Johnson, K., Fagan, A., Gill, M., Meaney, J., Frodl, T., 2013. Attention network hypoconnectivity with default and affective network hyperconnectivity in adults diagnosed with attention-deficit/hyperactivity disorder in childhood. *JAMA Psychiatry* 70, 1329–1337.
- Miikkulainen, R., 2021. Creative AI through evolutionary computation: Principles and examples. *SN Comput Sci* 2, 163.
- Ongür, D., Lundy, M., Greenhouse, I., Shinn, A.K., Menon, V., Cohen, B.M., Renshaw, P.F., 2010. Default mode network abnormalities in bipolar disorder and schizophrenia. *Psychiatry Res.* 183, 59–68.
- Park, B.-Y., Hong, S.-J., Valk, S.L., Paquola, C., Benkarim, O., Bethlehem, R.A.I., Di Martino, A., Milham, M.P., Gozzi, A., Yeo, B.T.T., Smallwood, J., Bernhardt, B.C., 2021. Differences in subcortico-cortical interactions identified from connectome and microcircuit models in autism. *Nat. Commun.* 12, 2225.
- Perry, A., Roberts, G., Mitchell, P.B., Breakspear, M., 2019. Connectomics of bipolar disorder: a

- critical review, and evidence for dynamic instabilities within interoceptive networks. *Mol. Psychiatry* 24, 1296–1318.
- Poldrack, R.A., Congdon, E., Triplett, W., Gorgolewski, K.J., Karlsgodt, K.H., Mumford, J.A., Sabb, F.W., Freimer, N.B., London, E.D., Cannon, T.D., Bilder, R.M., 2016. A phenotype-wide examination of neural and cognitive function. *Sci Data* 3, 160110.
- Schirner, M., McIntosh, A.R., Jirsa, V., Deco, G., Ritter, P., 2018. Inferring multi-scale neural mechanisms with brain network modelling. *eLife* 7. <https://doi.org/10.7554/eLife.28927>
- Sharpe, D., 2015. Chi-Square Test is Statistically Significant: Now What? <https://doi.org/10.7275/TBFA-X148>
- Smith, R.E., Tournier, J.-D., Calamante, F., Connelly, A., 2013. SIFT: Spherical-deconvolution informed filtering of tractograms. *Neuroimage* 67, 298–312.
- Smith, R.E., Tournier, J.-D., Calamante, F., Connelly, A., 2012. Anatomically-constrained tractography: improved diffusion MRI streamlines tractography through effective use of anatomical information. *Neuroimage* 62, 1924–1938.
- Tournier, J.-D., Calamante, F., Connelly, A., 2007. Robust determination of the fibre orientation distribution in diffusion MRI: non-negativity constrained super-resolved spherical deconvolution. *Neuroimage* 35, 1459–1472.
- Tournier, J.-D., Smith, R., Raffelt, D., Tabbara, R., Dhollander, T., Pietsch, M., Christiaens, D., Jeurissen, B., Yeh, C.-H., Connelly, A., 2019. MRtrix3: A fast, flexible and open software framework for medical image processing and visualisation. *Neuroimage* 202, 116137.
- Tustison, N.J., Avants, B.B., Cook, P.A., Zheng, Y., Egan, A., Yushkevich, P.A., Gee, J.C., 2010. N4ITK: improved N3 bias correction. *IEEE Trans. Med. Imaging* 29, 1310–1320.
- van Ewijk, H., Heslenfeld, D.J., Zwiers, M.P., Buitelaar, J.K., Oosterlaan, J., 2012. Diffusion tensor imaging in attention deficit/hyperactivity disorder: a systematic review and meta-analysis. *Neurosci. Biobehav. Rev.* 36, 1093–1106.
- Wang, P., Kong, R., Kong, X., Liégeois, R., Orban, C., Deco, G., van den Heuvel, M.P., Thomas Yeo, B.T., 2019. Inversion of a large-scale circuit model reveals a cortical hierarchy in the dynamic resting human brain. *Sci. Adv.* 5, eaat7854.
- Whitfield-Gabrieli, S., Ford, J.M., 2012. Default mode network activity and connectivity in psychopathology. *Annu. Rev. Clin. Psychol.* 8, 49–76.
- Wilson, H.R., Cowan, J.D., 1972. Excitatory and inhibitory interactions in localized populations of model neurons. *Biophys. J.* 12, 1–24.
- Wong, K.-F., Wang, X.-J., 2006. A recurrent network mechanism of time integration in perceptual decisions. *J. Neurosci.* 26, 1314–1328.
- Xia, C.H., Ma, Z., Ceric, R., Gu, S., Betzel, R.F., Kaczkurkin, A.N., Calkins, M.E., Cook, P.A., García de la Garza, A., Vandekar, S.N., Cui, Z., Moore, T.M., Roalf, D.R., Ruparel, K., Wolf, D.H., Davatzikos, C., Gur, R.C., Gur, R.E., Shinohara, R.T., Bassett, D.S., Satterthwaite, T.D., 2018. Linked dimensions of psychopathology and connectivity in functional brain networks. *Nat. Commun.* 9, 3003.
- Yang, G.J., Murray, J.D., Wang, X.-J., Glahn, D.C., Pearlson, G.D., Repovs, G., Krystal, J.H., Anticevic, A., 2016. Functional hierarchy underlies preferential connectivity disturbances in schizophrenia. *Proc. Natl. Acad. Sci. U. S. A.* 113, E219–28.
- Yeo, B.T.T., Krienen, F.M., Sepulcre, J., Sabuncu, M.R., Lashkari, D., Hollinshead, M., Roffman, J.L., Smoller, J.W., Zöllei, L., Polimeni, J.R., Fischl, B., Liu, H., Buckner, R.L., 2011. The organization of the human cerebral cortex estimated by intrinsic functional connectivity. *J. Neurophysiol.* 106, 1125–1165.
- Zhang, M., Sun, Y., Saggar, M., 2022. Cross-attractor repertoire provides new perspective on structure-function relationship in the brain. *Neuroimage* 259, 119401.